



Synthesis, spectral, thermal, structural, optical characterization, and Hirshfeld surface analysis of *N,N'*-diethylnicotinamide complexes of Mn(II) and Co(II) 4-cyanobenzoates

Mustafa Sertçelik¹ · Füreyâ Elif Özbek¹ · Mustafa Yüksek² · Ayhan Elmalı³ · Ömer Aydoğdu⁴ · Hacali Necefoğlu^{4,5} · Tuncer Hökelek⁶

Received: 17 September 2019 / Accepted: 23 December 2019 / Published online: 8 January 2020
© Institute of Chemistry, Slovak Academy of Sciences 2020

Abstract

Two new complexes, $[M(4\text{-CNB})_2(\text{DENA})_2(\text{H}_2\text{O})_2]$ (where M: Co and Mn, 4-CNB = 4-cyanobenzoate and DENA = *N,N'*-diethylnicotinamide), were synthesized and characterized using different techniques (elemental analysis, FT-IR Spectroscopy, single-crystal X-ray diffraction, and TGA/DTA analysis). Looking at the crystal structure of the complexes, the metal atoms are coordinated by two nitrogen atoms from two DENA ligands, two carboxyl oxygen atoms from two 4-cyanobenzoate anions, and two oxygen atoms from two water molecules, and the complexes have distorted octahedral geometry around the metal atom center. Both complexes were crystallized with the P-1 space group in the triclinic system. The linear absorption and emission features of the complexes were recorded by UV–Vis and fluorescence spectrophotometers, respectively. Linear absorption and emission results of the complexes showed that $[\text{Mn}(4\text{-CNB})_2(\text{DENA})_2(\text{H}_2\text{O})_2]$ complex can be used as optical filter below 400 nm wavelength when $[\text{Co}(4\text{-CNB})_2(\text{DENA})_2(\text{H}_2\text{O})_2]$ complex has a good application potential among the fluorescent materials, because of its high emission intensity. In addition, the Hirshfeld surfaces analyses of complexes have been investigated in detail.

Keywords Metal complex · 4-cyanobenzoic acid · *N,N'*-diethylnicotinamide · Optical characterization · X-ray diffraction · Hirshfeld surface analysis

Electronic supplementary material The online version of this article (<https://doi.org/10.1007/s11696-019-01040-0>) contains supplementary material, which is available to authorized users.

✉ Mustafa Sertçelik
mustafasertcelik@gmail.com

- ¹ Department of Chemical Engineering, Faculty of Engineering and Architecture, Kafkas University, 36300 Kars, Turkey
- ² Department of Electrical and Electronics Engineering, Faculty of Engineering and Architecture, Kafkas University, 36300 Kars, Turkey
- ³ Department of Physical Engineering, Faculty of Engineering, Ankara University, 06100 Ankara, Turkey
- ⁴ Department of Chemistry, Faculty of Sciences and Arts, Kafkas University, 36300 Kars, Turkey
- ⁵ International Scientific Research Centre, Baku State University, 1148 Baku, Azerbaijan
- ⁶ Department of Physics, Hacettepe University, 06800 Beytepe, Ankara, Turkey

Introduction

Metal complexes of aromatic carboxylic acids have attractive topological structures. These structures consist of metal atoms, coordinating with organic or inorganic ligands to form one-, two-, and three-dimensional network structures (Fujita et al. 1994; Guo-Qing et al. 2007; Yeşilel et al. 2011; Zhou and Li 2017; Das et al. 2019). Physical, chemical, and biological properties of all of the materials depend on the variety of the structures. Namely, the changing of the central metals and/or coordination ligands of the compounds leads to variation of the physical, chemical, and biological properties of the materials. In addition, the synthesis technique affects the structure of the compounds. For these reasons, aromatic carboxylic acids have wide scientific and technologic investigation areas (Szmigiel et al. 2018; Zhou et al. 2019). For several decades, scientists have studied the synthesis techniques, and magnetic and optical properties of 4-cyanobenzoic acid complexes (Li et al. 2006, 2007; Askin et al. 2015; Morales-Tapia et al. 2015; Akduran et al.

2016a, b, c; Ozbek et al. 2017). These complexes have potential technologic applications such as photodetector, gas adsorption materials, molecular sensor, catalyst materials, and chemical sensor (Allendorf et al. 2009; Coronado and Espallargas 2013; Mason et al. 2013; Uzun and Keskin 2014; Zhou et al. 2015; Altürk et al. 2015; Ghosh et al. 2016). The aromatic carboxylic acid derivatives which are consisted of transition metal and N- and O-donor ligands crystallize with wide variety of crystalline structures, and this property offers significant physical features for them. Furthermore, N- and O- donor atom involving ligands plays an important role in the biological system, and it shows anti-tumor, anti-fungal, and anti-bacterial activity behaviors (Meunier et al. 1983; Roy et al. 2010; Kose et al. 2014; Yıldırım et al. 2019). *N,N'*-diethylnicotinamide (DNA) is an key member of the so-called complex family (Bushma and Lukienko 1985; Smolkova et al. 2018).

As we mentioned above, the monomer, dimer, and trimer structures of the aromatic carboxylic complexes exhibit interesting photophysical behaviors. As a member of the carboxylic acid family, the benzoic acid complexes and their derivatives exhibit only phosphorescence behavior at monomer form, while they show both of fluorescence and phosphorescence behaviors at dimer form (Baum and McClure 1979). In a previous study, it was reported that the presence of the hydrogen bonding affects the linear optical absorption and fluorescence wavelengths of the benzoic acid derivatives (Baum and McClure 1979). Namely, the hydrogen bonding can be acting as donor or acceptor in the structure. Whether it behaves as a donor, the density of sigma bonds becomes dominant according to the pi bond density, on the contrary, if it behaves as acceptor the pi bonds density becomes dominant with respect to the sigma bond density. In case the existence of the acceptor hydrogen bonding, the organic complexes gain potential in organic light-emitting diode (OLED) applications. In our study, the ratio of the N- and O-donor atom bonds is more according to the H bonds. For these reasons, the dominant pi peaks have been expected in the emission spectra of the complexes. The emission features of these materials are also related to the used solvent types and solution concentrations (Kanda et al. 1963; Takeshita and Tsuji 1974). It is well known that the materials which have emission properties may create application opportunities as biosensors in immunology, DNA sequencing, optical sensor for the detection of nitroaromatic explosives, and protein interaction studies (Lakowicz 2006; Basabe-Desmonts et al. 2007; Caron et al. 2009; Muhammad et al. 2016).

In this study, two new metal complexes of Co(II) and Mn(II) 4-cyanobenzoates (4-CNB) with DNA were synthesized. The structures of the complexes were determined with the help of the X-ray diffraction technique, the FT-IR spectroscopy, and elemental analysis. The Optical and fluorescence features of the complexes were studied by UV-Vis

and fluorescence spectrophotometers, respectively. Thermal stabilities of the complexes were also investigated by TGA-DTA analysis. In addition, the Hirshfeld Surface Analysis was done to determinate the intermolecular interactions of the complexes.

Experimental

Synthesis of the complexes

All chemicals were high-purity products and used without any purification.

Synthesis of trans-diaquabis(4-cyanobenzoato- κ O)bis(*N,N*-diethylnicotinamide- κ N)-cobalt(II) (Complex 1)

In the Erlenmeyer flask, 4-cyanobenzoic acid (0.01 mol, 1.471 g) and sodium bicarbonate (0.01 mol, 0.84 g) were dissolved in 100 mL distilled water. As a result of the reaction, sodium 4-cyanobenzoate solution was obtained. $\text{CoSO}_4 \cdot 7\text{H}_2\text{O}$ (0.005 mol, 1.41 g) and DNA (0.01 mol, 1.78 g) in separate beakers were dissolved in 50 mL of distilled water. The solutions of DNA and sodium 4-cyanobenzoate were added to the CoSO_4 solution, respectively. The resulting clear solution was allowed to crystallize at room temperature. Pink single crystals were obtained after 1 week. The crystals were filtered off and washed with distilled water and dried at room temperature. Anal. Calcd. (%) for complex 1, $\text{C}_{36}\text{H}_{40}\text{CoN}_6\text{O}_8$ (MW = 743.68) C, 56.92; H, 5.10; N, 10.95. Found (%): C, 58.15; H, 5.34; N, 11.35. Yield 3.12 g (83.9%).

Synthesis of trans-diaquabis(4-cyanobenzoato- κ O)bis(*N,N*-diethylnicotinamide- κ N)-manganese(II) (complex 2)

The method employed for complex 1 was also used in complex 2. $\text{Mn}(\text{SO}_4) \cdot \text{H}_2\text{O}$ (0.005 mol 0.85 g) was used instead of $\text{CoSO}_4 \cdot 7\text{H}_2\text{O}$ and the final solution crystallized by the same method. The white crystals obtained were filtered off, washed with distilled water, and dried at room temperature. Anal. Calcd. (%) for complex 2, $\text{C}_{36}\text{H}_{40}\text{MnN}_6\text{O}_8$ (MW = 739.69) C, 57.95; H, 5.07; N, 11.06. Found (%): C, 58.48; H, 5.43; N, 11.35. Yield 2.56 g (69.2%).

Characterization of complexes

C, H, and N analyses were performed using Perkin Elmer LECO, CHNS-932 Elemental Analyser, and FT-IR spectra were recorded on an ALPHA-P BRUKER Spectrometer using in the range $4000\text{--}400\text{ cm}^{-1}$. The thermal properties

of the synthesized complexes were determined in the range of 10–1000 °C (heating rate 10 °C/min) using Shimadzu DTG 60 Thermal Analyzer. Philips PW 1830 was used for PXRD analysis.

Single-crystal X-ray diffraction analyses of complex **1** and **2** were performed on a Bruker APEX-II CCD diffractometer using Mo K α ($\lambda = 0.71073$ Å) radiation at a temperature of 296(2) K. Structures were solved by direct methods (Sheldrick 2008) and refined by full-matrix least squares against F^2 using all data (Sheldrick 2008). All non-H atoms were refined anisotropically. The water H atoms were located in difference Fourier maps and refined freely, while the C-bound H atoms were positioned geometrically at distances of 0.93 Å (for CH), 0.97 Å (for CH₂), and 0.96 Å (for CH₃) from the parent C atoms; a riding model was used during the refinement processes and the U_{iso} (H) values were constrained to be $U_{\text{iso}}(\text{H}) = k \times U_{\text{eq}}(\text{C})$, where $k = 1.2$ for aromatic CH and CH₂ and $k = 1.5$ for CH₃-H atoms. Experimental data are given in Table 1.

Hirshfeld surface analysis

To visualize the intermolecular interactions in the crystals of the complex, a Hirshfeld surface (HS) analysis (Hirshfeld 1977; Spackman et al. 2008) was carried out using *Crystal Explorer 17.5* (Turner et al. 2017).

The linear absorption and fluorescence measurements of the complexes

The complexes were dissolved in DMF solvent at 0.125 g/ml concentration and the absorption spectra of the solvents were recorded using a UV–Vis absorption spectrophotometer (*Shimadzu UV-1800*) versus a DMF-filled quartz cell as reference. In addition, the fluorescence (emission) properties of the complexes were investigated with help of fluorescence spectrophotometer (*Perkin Elmer LS55*) under 330 nm excitation wavelength. The complexes were excited at 5 nm intervals among 200 nm and 780 nm wavelengths, but the maximum fluorescence intensity was obtained under 330 nm excitation wavelength.

Table 1 Experimental details for complex **1** and **2**

	1	2
Empirical formula	C ₃₆ H ₄₀ CoN ₆ O ₈	C ₃₆ H ₄₀ MnN ₆ O ₈
Formula weight	743.68	739.69
Color/shape	Pink/prism	Colorless/block
Crystal system	Triclinic	Triclinic
Space group	<i>P</i> – <i>1</i>	<i>P</i> – <i>1</i>
<i>a</i> (Å)	7.4841 (2)	7.5038 (3)
<i>b</i> (Å)	8.5988 (3)	8.6620 (3)
<i>c</i> (Å)	15.0148 (5)	15.2190 (4)
α (°)	85.950 (4)	86.231 (4)
β (°)	75.935 (4)	75.728 (3)
γ (°)	74.204 (3)	74.537 (3)
<i>V</i> (Å ³)	901.89 (5)	923.97 (5)
<i>Z</i>	1	1
μ (Mo K α) (mm ^{−1})	0.54	0.42
ρ (calcd) (mg m ^{−3})	1.369	1.329
Number of reflections total	28,184	27,494
Number of reflections unique	3700	4573
R_{int}	0.051	0.027
$2\theta_{\text{max}}$ (°)	53.0	56.8
$T_{\text{min}}/T_{\text{max}}$	0.693/0.745	0.900/0.925
Number of parameters	242	242 242
GOF	1.05	1.08
$R [F^2 > 2\sigma(F^2)]$	0.050	0.034
wR	0.154	0.154 0.088
$(\Delta\rho)_{\text{max}}$ (e Å ^{−3})	1.346	0.24
$(\Delta\rho)_{\text{min}}$ (e Å ^{−3})	−0.47	−0.33

Results and discussion

Crystal structure

The X-ray structural determinations of complex 1 and 2 confirm the assignments of their structures from spectroscopic data. Selected bond lengths and angles are given in Table 2. Hydrogen-bond geometries are provided in Table 3. The molecular structures along with the atom-numbering schemes are depicted in Fig. 1a and b, while the partial packing diagrams are shown in Fig. 2a and b.

The asymmetric units of the crystal structures of the mononuclear complexes (1 and 2) contain metal (M) cations, Co1 (for 1) and Mn1 (for 2), located on inversion centres, one 4-CNB anion and one DENA molecule together with the one water molecule, with all ligands coordinating to M cations in monodentate manners (Fig. 1a, b).

Table 2 Selected bond lengths (Å) and angles (°) for complex (1 and 2)

Complex 1		Complex 2	
Co1–O2	2.0750 (19)	Mn1–O2	2.1402 (9)
Co1–O4	2.118 (2)	Mn1–O4	2.2157 (10)
Co1–N1	2.158 (2)	Mn1–N1	2.2820 (10)
O1–C1	1.245 (4)	O1–C1	1.2524 (17)
O2–C1	1.263 (4)	O2–C1	1.2674 (16)
O3–C14	1.232 (4)	O3–C14	1.236 (9)
N2–C14	1.338 (4)	N2–C14	1.3406 (18)
O2–Co1–O4	90.16 (9)	O2–Mn1–O4	92.47 (4)
O2–Co1–O4 ⁱ	89.84 (9)	O2–Mn1–O4 ⁱ	87.53 (4)
O2–Co1–N1	87.89 (8)	O2–Mn1–N1	92.48 (4)
O2–Co1–N1 ⁱ	92.11 (8)	O2–Mn1–N1 ⁱ	87.52 (4)
O4–Co1–N1 ⁱ	86.96 (9)	O4–Mn1–N1 ⁱ	91.87 (4)
O4 ⁱ –Co1–N1 ⁱ	93.04 (9)	O4 ⁱ –Mn1–N1 ⁱ	88.13 (4)
O1–C1–O2	125.6 (3)	O1–C1–O2	126.15 (12)

Symmetry codes: (i) $-x, -y, -z$

Table 3 Hydrogen-bond geometry (Å, °) for complex (1 and 2)

Complex	D–H...A	D–H	H...A	D...A	D–H...A
1	O4–H41...O3 ⁱ	0.82 (4)	2.05 (4)	2.823 (3)	157 (4)
	O4–H42...O1 ⁱⁱ	0.85 (6)	1.80 (6)	2.631 (3)	166 (5)
	C4–H4...Cg2 ⁱⁱⁱ	0.93	3.225	3.918 (3)	133
2	O4–H41...O1 ⁱⁱ	0.94 (2)	1.73 (2)	2.6482 (16)	163 (2)
	O4–H42...O3 ^{iv}	0.81 (2)	2.00 (2)	2.8080 (17)	172 (2)
	C4–H4...Cg2 ^v	0.93	3.249	3.927 (2)	132

Symmetry codes: (1) $-x+1, -y-1, -z$; (2) $-x, -y, -z$; (3) $-1+x, y, z$; (4) $x+1, y-1, z$; (5) $1-x, -y, -z$. Cg2 is the centroid of pyridine B (N1/C9–C13) ring

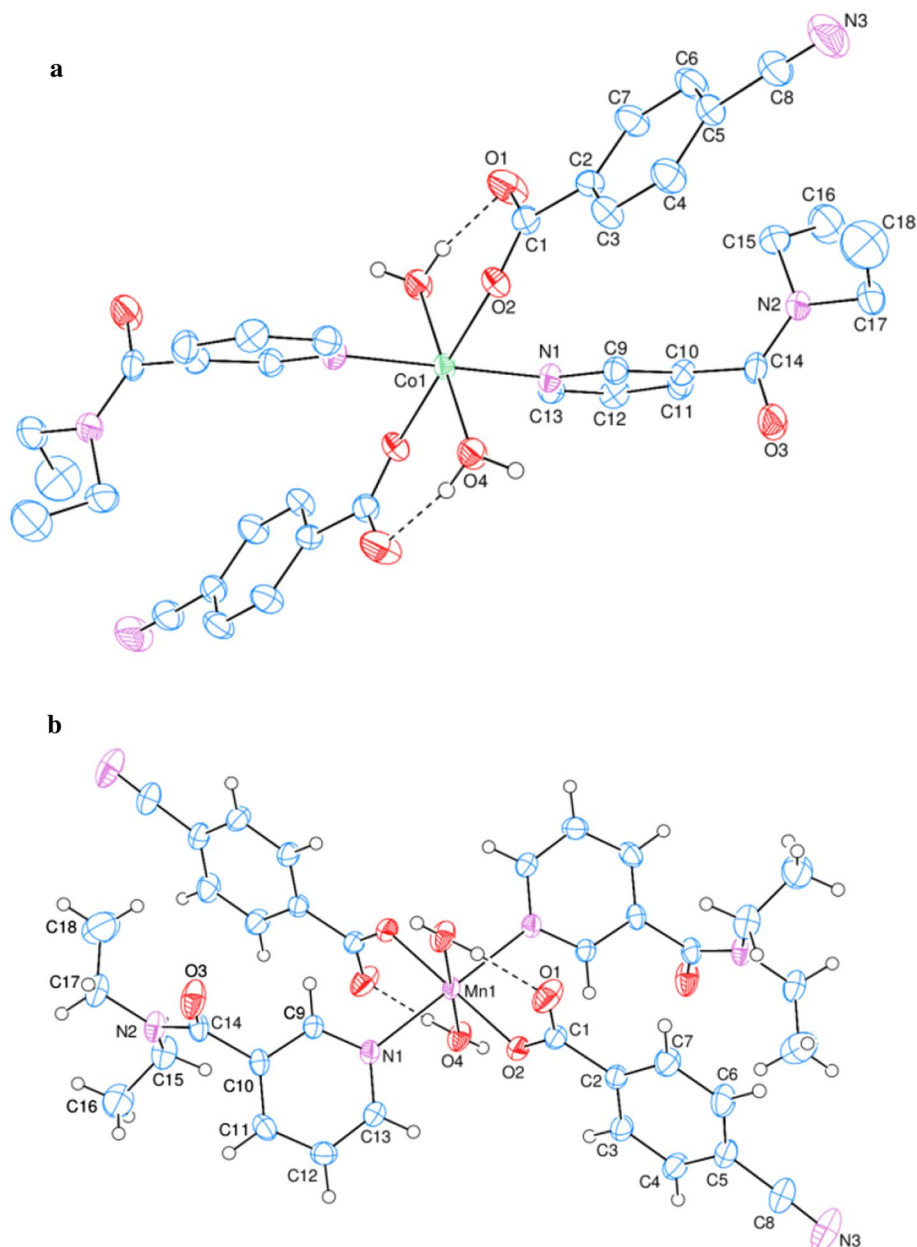
The M cations are coordinated monodentately through the two carboxylate O atoms (O2 and O2ⁱ) of the two symmetry-related 4-CNB anions and the two symmetry-related water O atoms (O4 and O4ⁱ) at distances of [2.0750 (19) and 2.118 (2) Å (for 1)] and [2.1402 (9) and 2.2157 (10) Å (for 2)], respectively, to form slightly distorted square-planar arrangements, while the slightly distorted octahedral coordination spheres are completed by the two symmetry-related N atoms (N1 and N1ⁱ) at distances of [2.158 (2) Å (for 1) and 2.2820 (10) Å (for 2)] of the two symmetry-related DENA ligands in the axial positions [symmetry code: (i) $-x, -y, -z$] (Fig. 1a, b).

The near equalities of the C1–O1 [1.245 (4) Å (for 1) and 1.2524 (17) Å (for 2)] and C1–O2 [1.263 (4) Å (for 1) and 1.2674 (16) Å (for 2)] bonds in the carboxylate groups indicate delocalized bonding arrangements, rather than localized single and double bonds. The M–O bond lengths [2.118 (2) Å (for 1) and 2.2157 (10) Å (for 2)] for water oxygen atoms are by ca 0.043 Å (for 1) 0.076 Å (for 2) longer than those the benzoate oxygen atoms [2.0750 (19) Å (for 1) and 2.1402 (9) Å (for 2)]. The M–N bond lengths [2.158 (2) Å (for 1) and 2.2820 (10) Å (for 2)] are the longest ones in the MO₄N₂ octahedrons. The metal atoms lie 0.7251(1) Å (for 1) and 0.7099(1) Å (for 2) below the planar (O1/O2/C1) carboxylate groups. The O1–C1–O2 bond angles [125.6 (3)° (for 1) and 126.15 (12)° (for 2)] seem to be significantly increased than that present in a free acid [122.2°]. The O–M–O and O–M–N bond angles [range 86.96 (9) to 93.04 (9)° (for 1) and 87.52 (4) to 92.47 (4)° (for 2) for *cis* angles; all *trans* angles are 180° due to symmetry] deviate slightly from ideal values, with the same average values of 90.00(9)° (for 1) and 90.00(4)° (for 2).

The dihedral angles between the planar carboxylate groups (O1/O2/C1) and the adjacent benzene A (C2–C7) rings are 8.98 (26)° (for 1) and 10.27 (12)° (for 2), while the benzene and pyridine B (N1/C9–C13) rings are oriented at dihedral angles of A/B = 56.18 (9)° (for 1) and 57.48(4)° (for 2).

In both complex (1 and 2), the intramolecular O–H_w...O_c (w = water, c = non-coordinating carboxylate O atom) hydrogen bonds (Table 1) link two of the water ligands to the 4-CNB anions, enclosing S(6) ring motifs (Bernstein et al. 1995) (Fig. 1a, b). The other water H atom is involved in intermolecular O–H_w...O_{DENA} (O_{DENA} = carbonyl O atom of the *N,N*-diethylnicotinamide) hydrogen bonds (Table 1), leading to the formations of layers parallel to (110) through the R₂²(16) ring motifs (Bernstein et al. 1995) (Fig. 2a, b). The π ... π interactions between the pyridine B (N1/C9–C13) rings, Cg2–Cg2ⁱ [symmetry codes: (i) $-x, 1-y, -z$, where Cg2 is the centroid of ring B] may further stabilize the structures with the centroid–centroid distances of 3.492(2) Å (for 1) and 3.510 (1) Å (for 2). There are also weak C–H... π interactions (Table 3).

Fig. 1 An ORTEP-3 (Farrugia 2012) view of **a** complex **1** and **b** complex **2**. The thermal ellipsoids are drawn at the 40% probability level. Intramolecular O–H_w⋯O_c (w = water, c = non-coordinating carboxylate O atom) hydrogen bonds are shown as dashed lines. Non-bonding hydrogen atoms have been omitted for clarity



FT-IR analysis

The severe and wide band, located around 3500–2900 cm^{-1} for OH-stretching vibration, indicates the presence of coordinated water molecules in complexes. The Δ value, that is the difference between asymmetric and symmetric stretching frequencies ($\nu_{\text{as}}(\text{COO}^-)$ and $\nu_{\text{s}}(\text{COO}^-)$) is known to estimate the coordination types of the carboxylate group. These values for complex 1 and complex 2 were calculated $\Delta\nu$ 164 and $\Delta\nu$ 169, respectively. A higher $\Delta\nu$ value than that of the sodium 4-cyanobenzoate salt indicates that the carboxylate group is monodentate coordinated. (Nakamoto 2006). For both complexes, the cyano $\nu(\text{C}\equiv\text{N})$ -stretching vibration

gives a sharp peak at the same frequency, ca. 2230 cm^{-1} , as noted for the free 4-CNB ligand, indicating that the cyano group is not coordinated (Nakamoto 2006; Ozbek et al. 2017). The vibrations of the pyridine ring of DENA in 1680–1630 cm^{-1} shift to low frequencies in the spectrum of metal complexes (Köse et al. 2012). The selected FT-IR spectrum peaks of the complex are listed in Table 4. FT-IR spectra of the complexes are shown in S1 and S2.

Thermogravimetric analysis

The thermal decomposition curves of complex 1 and complex 2 are shown in S3 and S4. The thermal decomposition

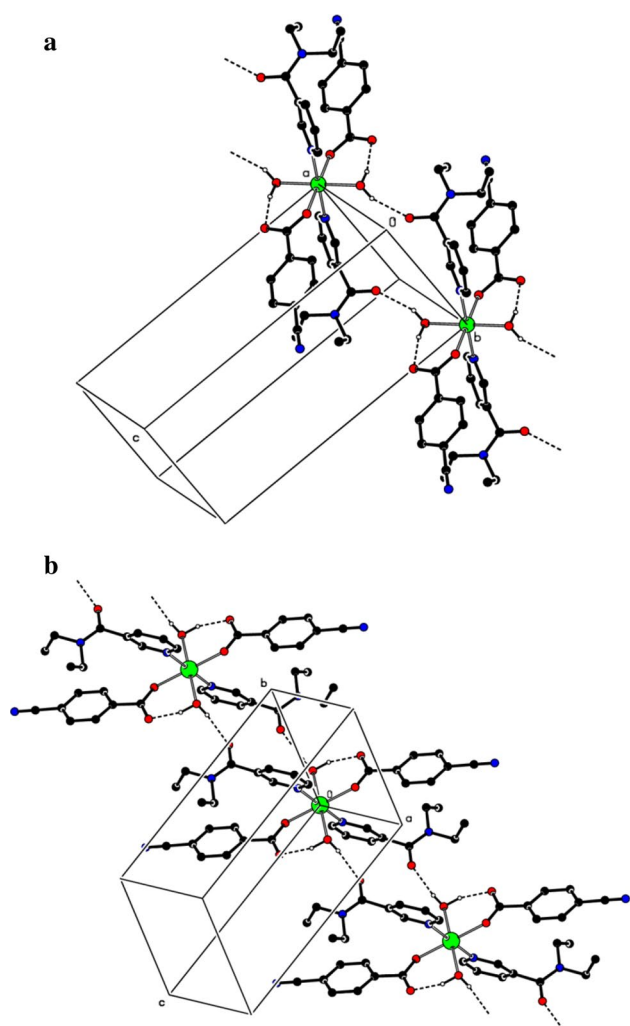


Fig. 2 A partial packing diagram of **a** complex 1 and **b** complex 2. Intramolecular $\text{O-H}_w \cdots \text{O}_c$ (w = water, c = non-coordinating carboxylate O atom) and intermolecular $\text{O-H}_w \cdots \text{O}_{\text{DENA}}$ (O_{DENA} = carbonyl O atom of the *N,N*-diethylnicotinamide) hydrogen bonds are shown as dashed lines. Non-bonding H atoms have been omitted for clarity

Table 4 Selected FT-IR spectrum peaks of the complexes

Groups	Complex 1	Complex 2
$\nu(\text{OH})_{\text{H}_2\text{O}}$	3422	3410
$\nu(\text{C-H})_{\text{aromatik}}$	2977	2975
$\nu(\text{C}\equiv\text{N})$	2228	2227
$\nu(\text{C}=\text{O})_{\text{amide}}$	1600	1598
$\nu_{\text{as}} \text{COO}^-$	1540	1543
$\nu_{\text{s}} \text{COO}^-$	1375	1374
$\Delta\nu$	164	169
$\nu(\text{M-N})$	785	566
$\nu(\text{M-O})$	785	564

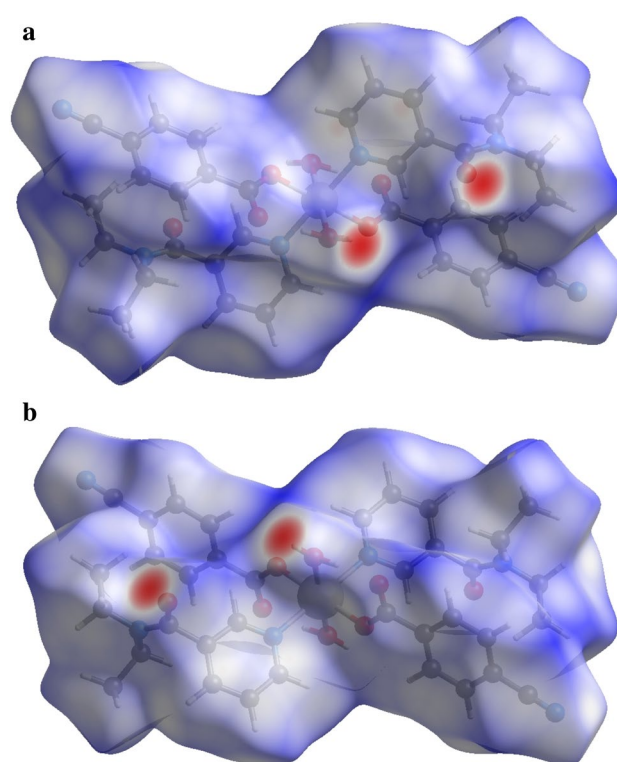


Fig. 3 **a** View of the three-dimensional Hirshfeld surface of complex 1 and plotted over d_{norm} in the range -0.5531 to 1.5746 a.u. **b** View of the three-dimensional Hirshfeld surface of complex 2 and plotted over d_{norm} in the range -0.6019 to 1.6854 a.u.

of the complexes started by losing two moles of hydrate water at 100 – 160 °C (complex 1) and 100 – 140 °C (complex 2), respectively. In both complexes, two coordinated water was dehydrated in the first step, giving an endothermic DTA peak at 130 °C and 108 °C, respectively (complex 1; exp. 4.8% , calc. 4.8% , complex 2; exp. 4.7% ; calc. 4.80%). In the following steps, organic ligands were beginning to decompose. When the thermal decomposition was completed, the final products were determined as CoO (complex 1; exp. 91.4% , calc. 89.9%) and MnO (complex 2; exp. 89.8% , calc. 90.4%) (Findoráková et al. 2010; Yıldırım et al. 2019).

Hirshfeld surface analysis

The contacts with distances equal to the sum of van der Waals radii, shorter (in close contact) and longer (distinct contact) than van der Waals radii are represent as white, red, and blue, respectively, in the HS plotted over d_{norm} (Fig. 3a [for 1] and b [for 2]) (Venkatesan et al. 2016).

The dominant interactions between $\text{O-H}_w \cdots \text{O}_{\text{DENA}}$ hydrogen bonds due to the near O3 and water hydrogen atoms (H41 and/or H42) can be seen as the bright-red spots, and are acted as the donors and/or acceptors (Table 1). They also appear as blue and red regions, corresponding

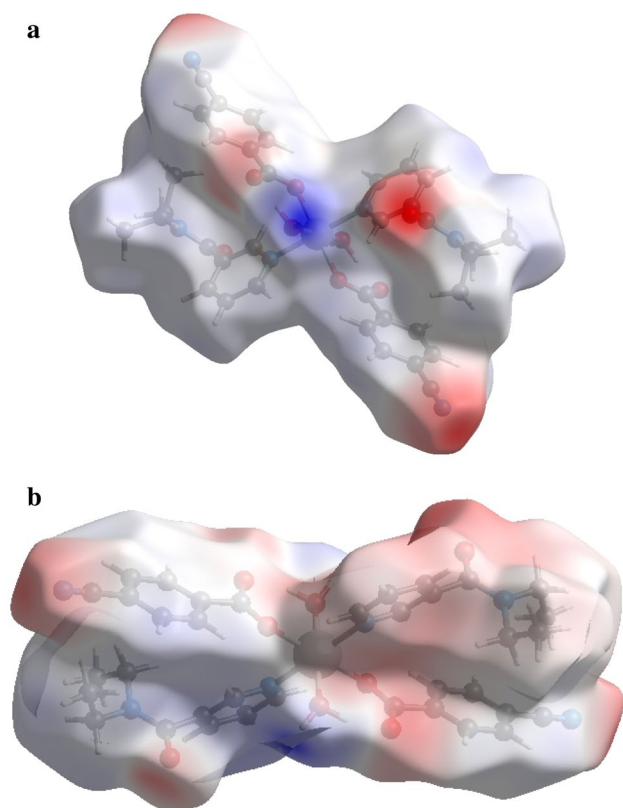


Fig. 4 **a** View of the three-dimensional Hirshfeld surface of complex **1** and complex plotted over electrostatic potential energy in the range -0.0923 to 0.1727 a.u. using the STO-3G basis set at the Hartree–Fock level of theory which hydrogen-bond donors and acceptors are shown as blue and red regions around the atoms corresponding to positive and negative potentials, respectively **b** View of the three-dimensional Hirshfeld surface of complex **2** and complex plotted over electrostatic potential energy in the range -0.1235 to 0.1908 a.u. using the STO-3G basis set at the Hartree–Fock level of theory which hydrogen-bond donors and acceptors are shown as blue and red regions around the atoms corresponding to positive and negative potentials, respectively

to positive and negative potentials on the HS mapped over electrostatic potential (Jayatilaka et al. 2005; Spackman et al. 2008) as shown in Figs. 4a (for 1) and b (for 2). The positive electrostatic potential (hydrogen-bond donors) and the negative electrostatic potential (hydrogen-bond acceptors) correspond to blue and red regions, respectively. The presence of adjacent red and blue triangles which are estimated from Hirshfeld surfaces analyses is evidenced the π – π stacking interactions. As clearly shown in Fig. 5a (for 1) and b (for 2), π – π interactions can be seen for both of the synthesized complexes.

The overall two-dimensional fingerprint plots, (Figs. 6a [for 1] and 7a [for 2]), and those delineated into H...H, H...O/O...H, H...N/N...H, H...C/C...H, C...C, N...C/C...N, O...O, and O...C/C...O contacts (McKinnon et al. 2007) are illustrated in Figs. 6b–i (for 1) and 7b–i (for 2) together with their

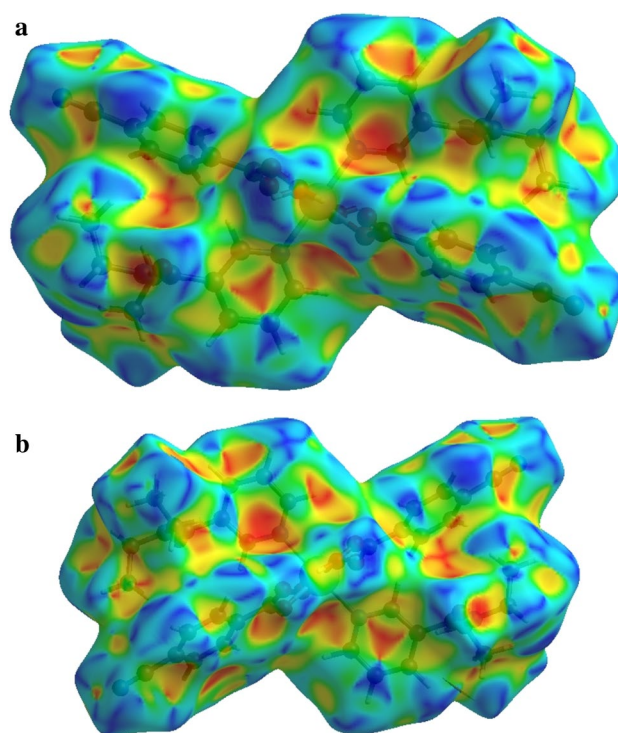


Fig. 5 Hirshfeld surface of **a** complex **1** and **b** complex **2** plotted over shape-index

relative contributions to the Hirshfeld surface. The most important interactions are H...H contributing 45.6% (for 1) and 46.3% (for 2) to the overall crystal packings, which are reflected in Figs. 6b (for 1) and 7b (for 2) as widely scattered points of high density due to the large hydrogen contents of the molecules. The wide spikes with the tips at $d_e = d_i = 2.20$ Å (for 1) and 2.25 Å (for 2) in Figs. 6b (for 1) and 7b (for 2) are due to the short interatomic H...H contacts (Table 5). The pair of characteristic wings resulting in the fingerprint plots delineated into H...O/O...H contacts (Fig. 6c [for 1] and 7c [for 2]), the 19.3% (for 1), and 18.8% (for 2) contributions to the HS arise from the O–H...O hydrogen bonds (Table 3) as well as from the H...O/O...H contacts (Table 5) and are viewed as pair of spikes with the tips at $d_e + d_i = 1.87$ Å (for 1) and 1.80 Å (for 2). The H...N/N...H, (Figs. 6d [for 1] and 7d [for 2]) contacts (Table 5) in the structure with 15.2% (for 1 and 2) contributions to the HS have symmetrical distributions of points, and the pairs of spikes at $d_e + d_i = 2.64$ Å (for 1) and 2.58 Å (for 2) result from the interatomic H...N/N...H contacts (Table 5). In the presence of C–H... π interactions, the pairs of the scattered points of wings resulting in the fingerprint plots delineated into H...C/C...H contacts with 14.7% (for 1) and 14.4% (for 2) contributions to the HS have nearly symmetrical distributions of points, (Figs. 6e [for 1] and 7e [for 2]), with the tips at $d_e + d_i = 2.86$ Å (for 1) and 2.84 Å (for 2), arising from the H...C/C...H contacts

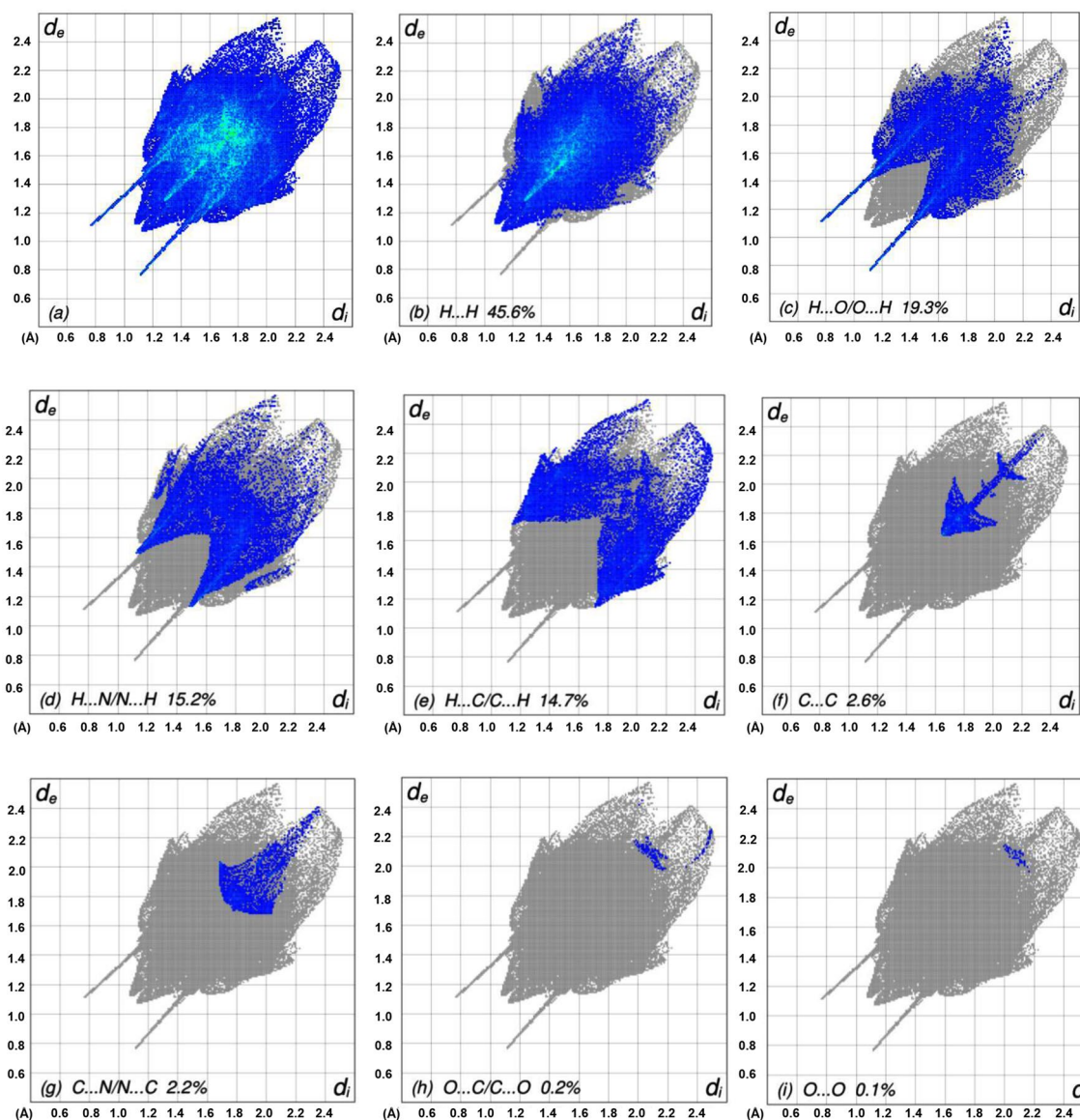


Fig. 6 The full two-dimensional fingerprint plots for complex **1**, showing **a** all interactions, and delineated into **(b)** H...H, **c** H...O/O...H, **d** H...N/N...H, **e** H...C/C...H, **f** C...C, **g** N...C/C...N, **h** O...O,

and **i** O...C/C...O interactions. The d_i and d_e values are the closest internal and external distances (in Å) from given points on the Hirshfeld surface contacts

(Table 5). Finally, the C...C (Figs. 6d [for 1] and 7d [for 2]) contacts (Table 5) in the structure with 2.6% (for 1 and 2) contributions to the HS have arrow-shaped distributions of points with the tips at $d_e + d_i = 1.65$ Å (for 1) and 1.67 Å (for 2), result from the interatomic C...C contacts (Table 5).

The Hirshfeld surface analysis confirms the importance of H-atom contacts in establishing the packings. The large number of H...H, H...O/O...H, H...N/N...H, and H...C/C...H interactions suggest that van der Waals interactions and hydrogen bonding play the major roles in the crystal packings (Hathwar et al. 2015).

The linear absorption and fluorescence results of the complexes

The recorded linear absorption traces of the ligands and complexes are given in Fig. 8. From the figure, it is clearly seen that the main linear absorption edges of the complexes start around 400 nm wavelength. In addition, the absorption edges of the complexes have shown red shift in the linear absorption spectra according to the absorption edges of the ligands. The red shift behaviors in the linear absorption spectra of the complexes are due to the non-covalent interactions which are weaker but strong

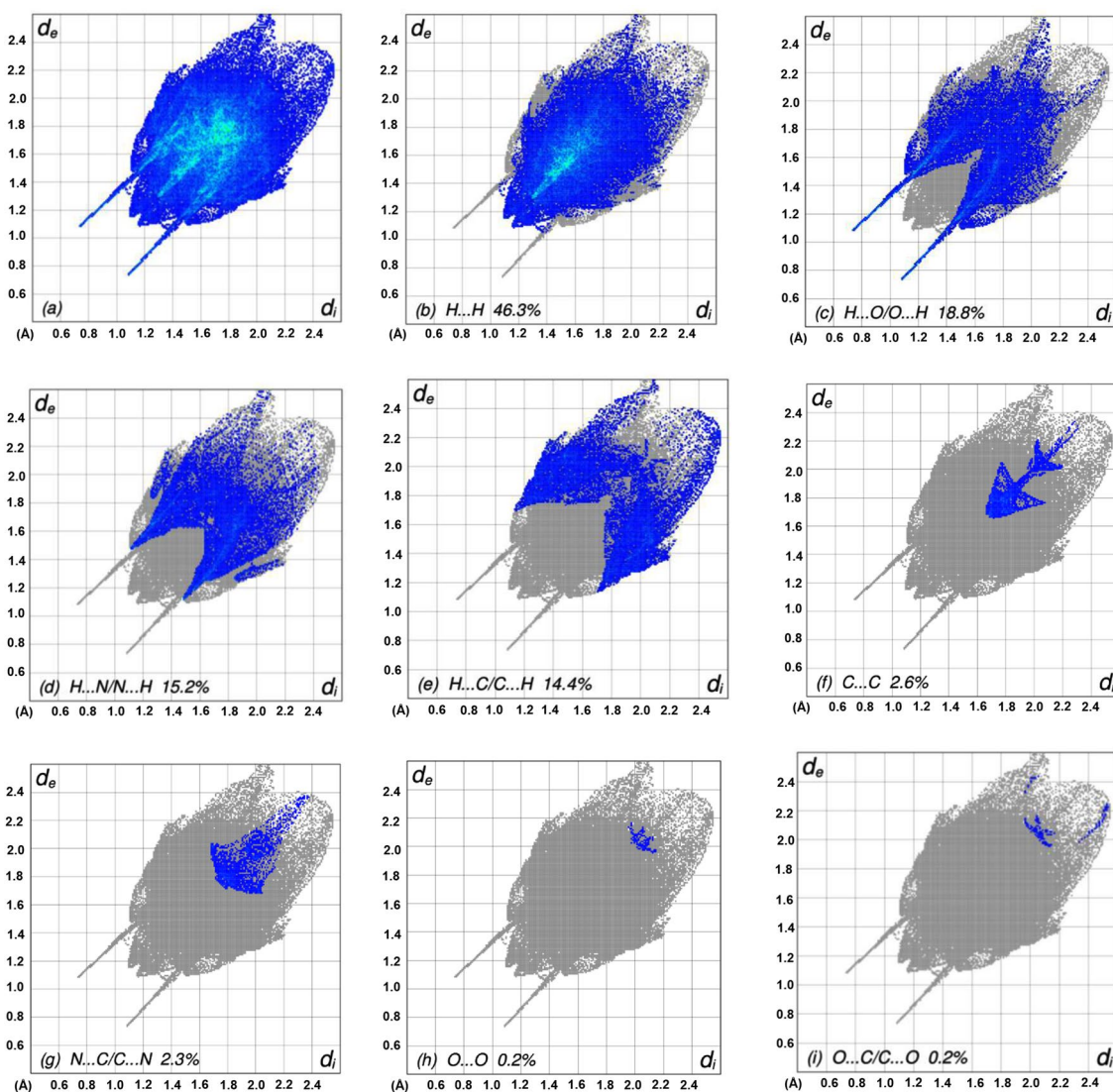


Fig. 7 The full two-dimensional fingerprint plots for complex **2**, showing **a** all interactions, and delineated into **b** H...H, **c** H...O/O...H, **d** H...N/N...H, **e** H...C/C...H, **f** C...C, **g** N...C/C...N, **h** O...O, and **i**

O...C/C...O interactions. The d_i and d_e values are the closest internal and external distances (in Å) from given points on the Hirshfeld surface contacts

than the covalent bonds, existing in the ligand structures. These linear absorptions are caused from the strong sigma bonds (Co–O, Co–N, O–C, and N–C for complex 1, and Mn–O, Mn–N, O–C, and N–C for complex 2) which correspond to near ultraviolet region of the electromagnetic spectra. In addition, complex 1 is showing a hump among 452 nm and 647 nm wavelengths. The hump is a result of the acceptor hydrogen bonds which are led to $n \rightarrow \pi^*$, $\pi \rightarrow n$, and $\pi \rightarrow \pi^*$ electronic transitions. As mentioned above in the single-crystal diffraction results (Table 3), the electronic transitions in the complex 1 are due to the O–H–O and C–H–C bonding. The complex 2 shows a small hump too, among 674 nm and 700 nm wavelengths. The electronic transitions contributed to the hump

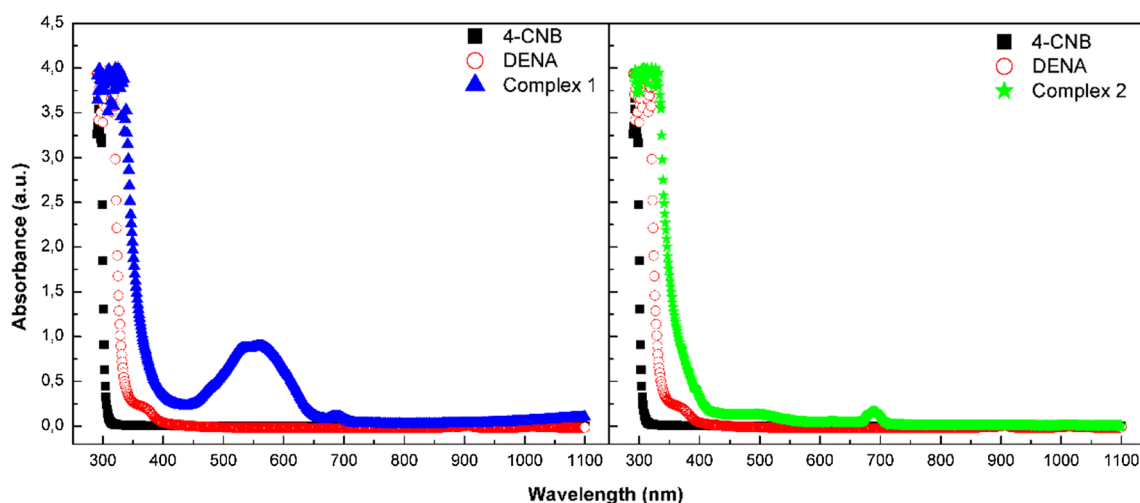
are consisted of the weak hydrogen bonds (C–H–C bonds, see Table 3). Here, the transitions become as $n \rightarrow \pi^*$.

The fluorescence spectra of the ligands and the complexes in DMF solvent at 0.125 g/l concentration are given in Fig. 9. The ligands exhibit fluorescence peaks around 400 nm wavelength. In addition, the complex 1 and complex 2 show emission peaks around 710 nm wavelength besides the emission peaks, causing from the ligands. The emission peaks which are taking place around 400 nm wavelength of the complexes have extinguished in intensity according to the emission peaks of the ligands. The complex 1 revealed two emission peaks among 388–476 nm and 678–761 nm wavelength ranges. The three emission peaks of the complex 2 appeared in 335–352 nm, 368–500 nm, and 673–760 nm

Table 5 Selected interatomic distances (Å) for complex (1 and 2)

Complex 1				Complex 2			
O1...C4 ⁱⁱ	3.363 (4)	C9...C12 ^x	3.462 (4)	O1...C4 ⁱⁱ	3.417 (2)	C9...C12 ^y	3.487 (2)
O1...O4 ⁱ	2.631 (3)	C10...C12 ^x	3.482 (4)	O1...O4 ⁱ	2.6482 (16)	C10...C12 ^y	3.5707 (19)
O3...O4 ⁱⁱⁱ	2.823 (3)	C10...C13 ^x	3.505 (4)	O3...O4 ⁱⁱⁱ	2.8080 (17)	C10...C13 ^y	3.5198 (18)
O4...C3 ^{iv}	3.383 (4)	C11...C15	3.356 (4)	O4...O1 ⁱ	2.6482 (16)	C11...C13 ^y	3.377 (2)
O1...H17B ^v	2.91	C11...C13 ^x	3.316 (4)	O4...O3 ^{iv}	2.8080 (17)	C11...C15	3.382 (2)
O1...H11 ^{vi}	2.88	C11...C12 ^x	3.588 (4)	O1...H11 ^v	2.77	C1...H9 ⁱ	2.99
O1...H7	2.51	C1...H9	2.95	O1...H7	2.51	C1...H41 ⁱ	2.43 (2)
O1H4 ⁱⁱ	2.66	C1...H42 ⁱ	2.45 (6)	O1...H41 ⁱ	1.73 (2)	C1...H11 ^v	2.99
O1...H42 ⁱ	1.80 (6)	C10...H15B	2.42	O1...H4 ⁱⁱ	2.73	C10...H15A	2.42
O2...H9	2.60	C11...H15B	2.74	O2...H9 ⁱ	2.64	C11...H15A	2.76
O2...H3	2.47	C15...H18C	2.89	O2...H3	2.47	C15...H18B	2.91
O2...H13 ⁱ	2.77	C16...H17A	2.71	O3...H17A	2.37	C16...H17B	2.73
O3...H12 ^{vii}	2.78	C16...H18A ⁱⁱ	2.97	O3...H9	2.92	C16...H18A ^{viii}	2.97
O3...H41 ⁱⁱⁱ	2.05 (4)	C17...H16C	2.80	O3...H12 ⁱⁱ	2.80	C17...H16B	2.84
O3...H17B	2.36	C18...H15A	2.80	O3...H42 ⁱⁱⁱ	2.00 (2)	C18...H15B	2.84
O3...H9	2.89	H15A...H18C	2.31	O4...H17A ^{iv}	2.90	H15B...H18B	2.34
O4...H3 ^{iv}	2.81	H16B...H18A ⁱⁱ	2.38	O4...H3 ^{vi}	2.88	H16B...H17B	2.22
O4...H17B ⁱⁱⁱ	2.86	H16C...H17A	2.18	N3...H16B ^{vii}	2.87	H16C...H18A ^{viii}	2.43
N3...H16A ^{vii}	2.93	H17B...H42 ⁱⁱⁱ	2.47	N3...H17B ^{vii}	2.70	H17A...H41 ⁱⁱⁱ	2.49
N3...H16C ^{viii}	2.85	C1...C9	3.287 (4)	C1...C9 ⁱ	3.3840 (19)	H17A...H42 ⁱⁱⁱ	2.52
N3...H17A ^{ix}	2.73						

Symmetry codes: [(1) $-x, -y, -z$; (2) $x-1, y, z$; (3) $-x+1, -y-1, -z$; (4) $-x+1, -y, -z$; (5) $x-1, y+1, z$; (6) $x, y+1, z$; (7) $x+1, y, z$; (8) $-x+2, -y-1, -z-1$; (7) $-x, -y-1, -z$ (for complex 1)] and [(1) $-x, -y, -z$; (2) $x-1, y, z$; (3) $x-1, y+1, z$; (4) $x+1, y-1, z$; (5) $-x, -y+1, -z$; (6) $-x+1, -y, -z$; (7) $x+2, y-1, z-1$; (8) $x+1, y, z$ (for complex 2)]

**Fig. 8** The linear absorption traces of the ligands and complexes in DMF solvent at room temperature

wavelength ranges. If the maximum fluorescence intensities of the complexes are compared, it can be easily calculated that the maximum fluorescence intensity of the complex 1 is nearly 9.1 times bigger than the maximum fluorescence intensity of the complex 2. The emissions of the complexes

which are taken place in the ultraviolet region can be attributed to the relaxations of the excited carriers among $\sigma^* \rightarrow \sigma$ and $\pi^* \rightarrow \pi$ states. In addition, the emissions of the complexes which are resulted in the visible region were estimated as the relaxation of the carriers among $\sigma^* \rightarrow n$ and

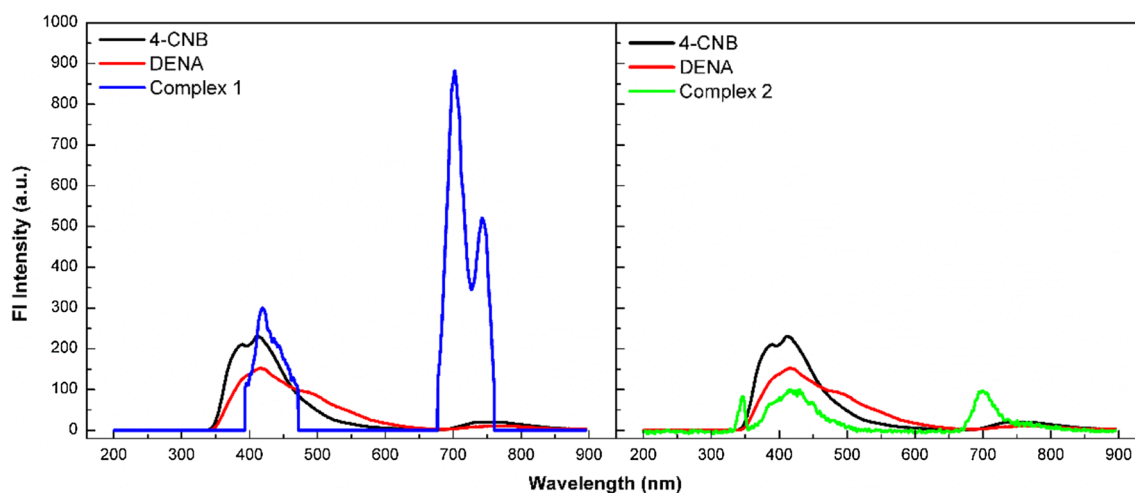


Fig. 9 The fluorescence spectra of the ligands and the complexes which are recorded at room temperature in DMF solution at 0.125 g/l concentration

$\pi^* \rightarrow n$ states. As a result, because of its high fluorescent intensity, the complex 1 has very good potential applications as fluorescent material.

XDR patterns of the complexes

The powder XRD patterns of complexes were measured over the $2\theta = 0\text{--}70^\circ$ range (in S5). When the X-ray diffractograms of the complexes 1 and 2 are examined, it is seen that they exhibit a similar pattern with a coincident overlap at 2θ values and d values. These coherent diffractograms revealed that the molecular arrangement of the ligands around the central metal atom and the geometry of the complexes were identical.

Conclusion

Structural conformation of complexes, bonding properties, and thermal decomposition steps has been studied. The metal:ligand:ligand rates of complexes were determined as 1:2:2. The geometry of both complex structures is distorted octahedral. The metal atoms are coordinated by two nitrogen atoms from two DENA ligands, two carboxyl oxygen atoms from two 4-CNB anions, and two oxygen atoms from two water molecules. The linear absorption spectra of the complexes has revealed that the absorption edges start from around 400 nm wavelength, and it corresponds to 3.10 eV in energy. The two emission peaks of the complex 1 have taken place in 388–476 nm and 678–761 nm wavelength ranges. The three emission peaks of the complex 2 have been located in 335–352 nm, 368–500 nm, and 673–760 nm wavelength ranges.

Supplementary data

Crystallographic data for the structural analysis have been deposited with the Cambridge Crystallographic Data Centre, CCDC 1,952,573–1,952,574 copies of this information may be obtained free of charge from The Director, CCDC, 12 Union Road, Cambridge CB2 1EZ, UK (fax: 44-1223-336033; e-mail: deposit@ccdc.cam.ac.uk or www: <http://www.ccdc.cam.ac.uk>).

Acknowledgements This research was supported by the Science Research Fund of Kafkas University (Project no: 2016-FM-49).

References

- Akduran N, Necefoglu H, Aydogdu O, Hokelek T (2016a) Crystal structure of catena-poly[[aquabis(4-cyanobenzoato-kappa O) copper(II)]-mu-N, N-diethyl-nicotinamide-kappa N-2(1):O]. Acta Crystallogr Sect E Crystallogr Commun 72:1183. <https://doi.org/10.1107/S205698901601183X>
- Akduran N, Necefoglu H, Aydogdu O, Hokelek T (2016b) Crystal structure of trans-diaquabis(4-cyanobenzoato-jO) bis(N, N-diethylnicotinamide-kappa N)zinc(II). Acta Crystallogr Sect E-Crystallogr Commun 72:1374. <https://doi.org/10.1107/S2056989016013815>
- Akduran N, Sertcelik M, Aydogdu O et al (2016c) Crystal structure of trans-diaquabis(4-cyanobenzoato-kappa O)bis(N, N-diethylnicotinamide-kappa N)cadmium. Acta Crystallogr Sect E-Crystallogr Commun 72:1827. <https://doi.org/10.1107/S2056989016018247>
- Allendorf MD, Bauer CA, Bhakta RK, Houk RJT (2009) Luminescent metal-organic frameworks. Chem Soc Rev 38:1330–1352. <https://doi.org/10.1039/B802352M>
- Altürk S, Tamer Ö, Avcı D, Atalay Y (2015) Synthesis, spectroscopic characterization, second and third-order nonlinear optical properties, and DFT calculations of a novel Mn(II) complex.

- J Organomet Chem 797:110–119. <https://doi.org/10.1016/j.jorganchem.2015.08.014>
- Askin GS, Nəcəföglü H, Nayir GY et al (2015) Crystal structure of trans-diaquabis(4-cyanobenzoato-kappa O)bis(nicotinamide-kappa N-1)cobalt(II). Acta Crystallogr Sect E-Crystallogr Commun 71:561. <https://doi.org/10.1107/S2056989015008270>
- Basabe-Desmonts L, Reinhoudt DN, Crego-Calama M (2007) Design of fluorescent materials for chemical sensing. Chem Soc Rev 36:993–1017. <https://doi.org/10.1039/b609548h>
- Baum J, McClure D (1979) Ultraviolet transitions of benzoic-acid. 1. Interpretation of the singlet absorption-spectrum. J Am Chem Soc 101:2335–2339. <https://doi.org/10.1021/ja00503a016>
- Bernstein J, Davis RE, Shimoni L, Chang N-L (1995) Patterns in hydrogen bonding: functionality and graph set analysis in crystals. Angew Chem Int Ed Engl 34:1555–1573. <https://doi.org/10.1002/anie.199515551>
- Bushma M, Lukienko P (1985) Interaction invitro of nicotinamide and diethylnicotinamide (cordiamine) with enzymes of rat-liver microsomal hydroxylating systems. Farmakol Toksikol 48:97–100
- Caron T, Guillemot M, Veignal F et al (2009) Optical sensor for the detection of explosives: example of a fluorescent material. In: Pardo M, Sberveglieri G (eds) Olfaction and electronic nose, proceedings. American Institute of Physics, Melville, p 83
- Coronado E, Espallargas GM (2013) Dynamic magnetic MOFs. Chem Soc Rev 42:1525–1539. <https://doi.org/10.1039/C2CS35278H>
- Das K, Datta A, Massera C, Sinha C (2019) Structural diversity, topology and luminescent properties of a two-dimensional Cd(II) coordination polymer incorporating 4,4'-dipyridyl and 4,4'-sulfonildibenzoic acid. J Mol Struct 1179:618–622. <https://doi.org/10.1016/j.molstruc.2018.11.051>
- Farrugia LJ (2012) WinGX and ORTEP for windows: an update. J Appl Crystallogr 45:849–854. <https://doi.org/10.1107/S0021889812029111>
- Findoráková L, Györyová K, Melník M et al (2010) Preparation, thermal decomposition, and crystal structure of Zn(II) 2-chlorobenzoate complex with nicotinamide. J Coord Chem 63:3348–3355. <https://doi.org/10.1080/00958972.2010.512083>
- Fujita M, Kwon YJ, Washizu S, Ogura K (1994) Preparation, clathration ability, and catalysis of a two-dimensional square network material composed of cadmium(II) and 4,4'-bipyridine. J Am Chem Soc 116:1151–1152. <https://doi.org/10.1021/ja00082a055>
- Ghosh S, Ganguly A, Bhattacharyya A et al (2016) Selective chromo-fluorogenic molecular sensor for dual channel recognition of Cu²⁺ and F⁻: effect of functional group on selectivity. RSC Adv 6:67693–67700. <https://doi.org/10.1039/C6RA09877K>
- Guo-Qing L, Yan L, Wen-Qiang Z et al (2007) One-dimensional supramolecular chain based on a dinuclear terbium(III) 4-cyanobenzoate complex. Chin J Struct Chem 26:805–810
- Hathwar VR, Sist M, Jørgensen MRV et al (2015) Quantitative analysis of intermolecular interactions in orthorhombic rubrene. IUCr J 2:563–574. <https://doi.org/10.1107/S2052252515012130>
- Hirshfeld FL (1977) Bonded-atom fragments for describing molecular charge densities. Theor Chim Acta 44:129–138. <https://doi.org/10.1007/BF00549096>
- Jayatilaka D, Grimwood DJ, Lee A et al (2005) TONTO—a system for computational chemistry. Available at: <http://hirshfeldsurface.net/>
- Kanda Y, Shimada R, Takenoshita Y (1963) The phosphorescence spectrum of benzoic acid, methyl benzoate and benzamide at 90°K. Spectrochim Acta 19:1249–1260. [https://doi.org/10.1016/0371-1951\(63\)80044-2](https://doi.org/10.1016/0371-1951(63)80044-2)
- Kose DA, Toprak E, Avci E et al (2014) Synthesis, spectral, thermal studies of Co(II), Ni(II), Cu(II) and Zn(II)-arginato complexes. crystal structure of monoaquabis(arginato-kappa O, kappa N) copper(II). [Cu(arg)(2)(H2O)]center dot NaNO3. J Chin Chem Soc 61:881–890. <https://doi.org/10.1002/jccs.201300351>
- Köse DA, Sahin O, Büyükgüngör O (2012) Synthesis, spectral, thermal, magnetic and structural study of diaquabis(m-hydroxybenzoato-kO)bis(N,N-diethylnicotinamide-kN)cobalt(II). Eur Chem Bull 1:196–201. <https://doi.org/10.17628/ecb.2012.1.196-201>
- Lakowicz JR (2006) Principles of fluorescence spectroscopy, 3rd edn. Springer, Cham
- Li Y, Zheng F-K, Liu X et al (2006) Crystal structures and magnetic and luminescent properties of a series of homodinuclear lanthanide complexes with 4-cyanobenzoic ligand. Inorg Chem 45:6308–6316. <https://doi.org/10.1021/ic0602603>
- Li Y, Li G-Q, Zheng F-K et al (2007) Synthesis, crystal structures and magnetic properties of three new 4-cyanobenzoate complexes. J Mol Struct 842:38–45. <https://doi.org/10.1016/j.molstruc.2006.12.013>
- Mason JA, Veenstra M, Long JR (2013) Evaluating metal-organic frameworks for natural gas storage. Chem Sci 5:32–51. <https://doi.org/10.1039/C3SC52633J>
- McKinnon JJ, Jayatilaka D, Spackman MA (2007) Towards quantitative analysis of intermolecular interactions with Hirshfeld surfaces. Chem Commun Camb Engl (Issue 37):3814–3816
- Meunier G, Meunier B, Auclair C et al (1983) Unexpected regioselective alkylation of the antitumor agent N2-methyl-9-hydroxyellipticinium acetate with N, O or S donors. Tetrahedron Lett 24:365–368. [https://doi.org/10.1016/S0040-4039\(00\)81408-2](https://doi.org/10.1016/S0040-4039(00)81408-2)
- Morales-Tapia AA, Colorado-Peralta R, Duarte-Hernandez AM et al (2015) Crystal structure of catena-poly[[[triacqua(4-cyanobenzoato-kappa O)nickel(II)]-mu-4,4'-bipyridine-kappa N-2: N'] 4-cyanobenzoate]. Acta Crystallogr Sect E-Crystallogr Commun 71:M197-U138. <https://doi.org/10.1107/S2056989015018344>
- Muhammad K, Nazir S, Hameed S, Bechtold IH (2016) Mesomorphic and fluorescence properties of methyl 4-(4-alkoxystyryl)benzoates. Liq Cryst 43:863–873. <https://doi.org/10.1080/02678292.2016.1148205>
- Nakamoto K (2006) Infrared and Raman spectra of inorganic and coordination compounds. Wiley, Hoboken, NJ
- Ozbek FE, Sertcelik M, Yuksek M et al (2017) Cu(II) and Ni(II) 4-cyanobenzoate complexes with nicotinamide: synthesis, structural and optical characterization and thermal behavior. J Mol Struct 1150:112–117. <https://doi.org/10.1016/j.molstruc.2017.08.074>
- Roy TG, Hazari SKS, Barua KK et al (2010) Synthesis, characterization and anti-microbial studies of cadmium(II) compounds containing 3,10-C-meso-Me-8[14]jane(C). Crystal and molecular structure of cis-[CdLC(NO3)](NO3). Appl Organomet Chem 24:878–887. <https://doi.org/10.1002/aoc.1703>
- Sheldrick GM (2008) A short history of SHELX. Acta Crystallogr A 64:112–122. <https://doi.org/10.1107/S0108767307043930>
- Smolkova R, Smolko L, Gyoryova K et al (2018) New zinc(II) 3-aminobenzoates with bioactive ligands: synthesis, thermal, spectral and antimicrobial properties. Thermochim Acta 669:1–7. <https://doi.org/10.1016/j.tca.2018.09.004>
- Spackman MA, McKinnon JJ, Jayatilaka D (2008) Electrostatic potentials mapped on Hirshfeld surfaces provide direct insight into intermolecular interactions in crystals. CrystEngComm 10:377–388. <https://doi.org/10.1039/B715227B>
- Szmigiel K, Nentwig M, Oeckler O et al (2018) Crystal structure, vibrational spectroscopic characterization, thermal behavior and antifungal activity of a novel coordination polymer of indole-3-carboxylic acid with cobalt(II) and a comparison with the isostructural Zn(II) complex. Inorg Chem Commun 97:56–62. <https://doi.org/10.1016/j.inoche.2018.09.009>
- Takeshita T, Tsuji K (1974) Electron-spin resonance study of photosensitized radical formation in N-hexane by benzoic-acid. J Phys Chem 78:105–107. <https://doi.org/10.1021/j100595a004>
- Turner MJ, McKinnon JJ, Wolff SK et al (2017) CrystalExplorer17, Univ West Aust. <http://hirshfeldsurface.net>

- Uzun A, Keskin S (2014) Site characteristics in metal organic frameworks for gas adsorption. *Prog Surf Sci* 89:56–79. <https://doi.org/10.1016/j.progsurf.2013.11.001>
- Venkatesan P, Thamotharan S, Ilangovan A et al (2016) Crystal structure, Hirshfeld surfaces and DFT computation of NLO active (2E)-2-(ethoxycarbonyl)-3-[(1-methoxy-1-oxo-3-phenylpropan-2-yl) amino] prop-2-enoic acid. *Spectrochim Acta A Mol Biomol Spectrosc* 153:625–636
- Yeşilel OZ, Ilker I, Şahin E (2011) One-dimensional Ni(II) and Cu(II) coordination polymers containing syn-syn thiophene-2,5-dicarboxylate and propane-1,3-diamine. *J Inorg Organomet Polym Mater* 21:103–109. <https://doi.org/10.1007/s10904-010-9414-1>
- Yıldırım T, Köse DA, Avcı E et al (2019) Novel mixed ligand complexes of acesulfame/nicotinamide with some transition metals. Synthesis, crystal structural characterization, and biological properties. *J Mol Struct* 1176:576–582. <https://doi.org/10.1016/j.molstruc.2018.08.099>
- Zhou Q-K, Li N-Y (2017) A three-dimensional cadmium coordination polymer based on 1,4-bis-(1,2,4-triazol-1-yl)but-2-ene and benzene-1,3,5-tri-carb-oxy-lic acid. *Acta Crystallogr Sect C Struct Chem* 73:749–753. <https://doi.org/10.1107/S2053229617012189>
- Zhou SY, Li X, Li T et al (2015) A series of heterospin complexes based on lanthanides and pyridine biradicals: synthesis, structure and magnetic properties. *RSC Adv* 5:17131–17139. <https://doi.org/10.1039/C4RA15074K>
- Zhou X, Liu K, Liu L et al (2019) Two 3-D metal organic frameworks based on pyridine carboxylic acid ligands with magnetism properties and photoluminescence. *Sci Adv Mater* 11:332–337. <https://doi.org/10.1166/sam.2019.3465>

Publisher's Note Springer Nature remains neutral with regard to jurisdictional claims in published maps and institutional affiliations.